Operator-based linearization approach for modeling of multiphase flow with buoyancy and capillarity

Lyu, Xiaocong; Khait, Mark; Voskov, Denis

DOI
10.2118/205378-PA

Publication date
2021

Document Version
Final published version

Published in
SPE Journal

Operator-Based Linearization Approach for Modeling of Multiphase Flow with Buoyancy and Capillarity

Xiaocong Lyu and **Mark Khait,** Delft University of Technology; and **Denis Voskov*,**
Delft University of Technology and Stanford University

Summary

Numerical simulation of coupled multiphase multicomponent flow and transport in porous media is a crucial tool for understanding and forecasting of complex industrial applications related to the subsurface. The discretized governing equations are highly nonlinear and usually need to be solved with Newton's method, which corresponds with high computational cost and complexity. With the presence of capillary and gravity forces, the nonlinearity of the problem is amplified even further, which usually leads to a higher numerical cost. A recently proposed operator-based linearization (OBL) approach effectively improves the performance of complex physical modeling by transforming the discretized nonlinear conservation equations into a quasilinear form according to state-dependent operators. These operators are approximated by means of a discrete representation on a uniform mesh in physical parameter space. Continuous representation is achieved through the multilinear interpolation. This approach provides a unique framework for the multifidelity representation of physics in general-purpose simulation. The applicability of the OBL approach was demonstrated for various energy subsurface applications with multiphase flow of mass and heat in the presence of buoyancy and diffusive forces. In this work, the OBL approach is extended for multiphase multicomponent systems with capillarity. Through the comparisons with a legacy commercial simulator using a set of benchmark tests, we demonstrate that the extended OBL scheme significantly improves the computational efficiency with the controlled accuracy of approximation and converges to the results of the conventional continuous approach with an increased resolution of parametrization.

Introduction

Numerical simulation, a tool developed by combining physics, mathematics, and computer programming, is an efficient way to understand the complex fluid flow in subsurface reservoirs with applications to the evaluation of hydrocarbon recovery, performance analysis, and various optimization problems (Todd et al. 1972; Spillette et al. 1973; Thomas and Thurnau 1983). It involves solving the partial-differential equations governing coupled multiphase flow and transport in porous media with highly nonlinear physics (Aziz and Settari 1979; Coats et al. 1995).

All coupled equations need to be discretized in space and time to solve the nonlinear system numerically. In reservoir simulation, the finite-volume-method discretization scheme has been widely used to discretize the mass-conservation equations in space (Aziz and Settari 1979; Edwards and Rogers 1998). Considering the stability of the solution, a fully implicit (backward-Euler) time discretization is more attractive to avoid restricted simulation timesteps (Peaceman 1977; Ewing 1991). In this approach, the elliptic flow and highly nonlinear hyperbolic transport problems cannot be decoupled (i.e., need to be solved simultaneously; Young and Russell 1993; Peaceman 2000). This process, however, introduces nonlinearity into the system of equations, which needs to be resolved by a nonlinear solver.

A Newton-based method is usually applied to linearize the coupled system of nonlinear equations, where an assembly of the Jacobian matrix and the residual vector is required. This is a difficult task in general-purpose reservoir simulation because both values and corresponding derivatives of different properties in the governing equations need to be evaluated and assembled at every nonlinear iteration (Cao 2002). The complexity of implementation also depends on the types of nonlinear unknowns and strategies that are used to perform the nonlinear update (Aziz and Wong 1989). For example, in compositional simulation, the natural formulation performs better for immiscible displacement, whereas the molar formulation shows better behavior for a miscible gasflooding (Voskov and Tchelepi 2012). In reality, strongly heterogeneous geological properties of the reservoir, such as porosity or permeability, can also increase the computational cost (Chang and Yortsos 1992).

Younis (2011) developed the Automatic Differentiation Expression Template Library to improve the robustness and flexibility of the linearization process. The Automatic Differentiation General Purpose Research Simulator, developed using the library, provides a flexible research platform for the implementation of advanced reservoir-simulation technologies (Zaydullin et al. 2016; Garipov et al. 2018). The nonlinear convergence for simulation problems involving complex physical phenomena such as gravity, capillarity, and chemical reactions still remains a challenging problem. Recently, several advanced nonlinear formulations were developed to successfully address these complex problems (Li and Tchelepi 2015; Hamon et al. 2018). However, most of the advanced nonlinear solvers for general-purpose simulation mentioned previously have been developed for natural formulation (Coats 1980) with explicit correction of saturation. An advanced simulation strategy for the molar formulation is still required to improve the convergence of the nonlinear solutions, especially in the presence of complex physical phenomena.

A new approach for the molar formulation called OBL, proposed by Voskov (2017), follows the ideas originated in Zaydullin et al. (2013). This approach presents a new way to linearize the governing equations compared with the conventional linearization approach. It is based on the transformation of the discretized mass-conservation equations to a combination of space-dependent and state-dependent operators. The first type of operators depends on the properties altered in space (e.g., porosity and permeability), while the second type relies on the physical properties of the rock and the fluid (e.g., density and viscosity). All those coefficients in the discretized mass-conservation equations that are fully defined by the physical state can be grouped together and represented as the state-dependent operators. At the linearization stage, the space-dependent operators are treated conventionally, while the state-dependent

*Corresponding author; email: D.V.Voskov@tudelft.nl

Original SPE manuscript received for review 26 September 2020. Revised manuscript received for review 18 December 2020. Paper (SPE 205378) peer approved 8 February 2021.

operators are approximated by discrete representation on a uniform mesh in the space of nonlinear unknowns. These state-dependent operators rely on local physical properties (e.g., density, viscosity, relative permeability), which often represent the most nonlinear part of governing equations. The continuous representation of operators is achieved through multilinear interpolation, which provides a unique tool for an efficient representation of the complex nonlinear physics of the simulation problem. The OBL approach also provides an opportunity to control the nonlinearity in physics by changing the resolution of parameter space, increasing performance, flexibility, and robustness of simulation (Khait and Voskov 2017).

The Delft Advanced Research Terra Simulator (DARTS), which is capable of modeling complex flow and transport related to various energy applications (Khait and Voskov 2017; Kala and Voskov 2020; Wang et al. 2020), is used to implement and test the proposed nonlinear formulation for multiphase multicomponent flow in the presence of gravity and capillarity. The OBL approach is deployed to resolve the highly nonlinear problems caused by those special physical phenomena. The main advantage of this approach is a simplified construction of the Jacobian matrix and residuals because the complex physics-based calculations (i.e., mainly related to the flux in the governing equations) are translated into generic multilinear interpolation according to supporting points that are used to store the values of state-dependent operators (Khait and Voskov 2018a). Meanwhile, the implementation of the fully implicit simulation code is significantly simplified with the OBL methodology. The discretized partial-differential equations and property evaluations are completely separated from each other. That simplifies the efficient, architecture-oriented implementation of advanced numerical approaches exploiting coarse-grained and fine-grained parallelism on central processing unit (CPU) and graphics processing unit (GPU), respectively (Khait et al. 2020). It is combined with high flexibility of the simulation code: direct implementation of all properties in Python has a minimal effect on simulation performance. To maintain high efficiency for large heterogeneous problems, the linear system is solved using flexible GMRES (Saad and Schultz 1986; Saad 1993) with the constrained pressure residual preconditioner (Wallis et al. 1985). The algebraic multigrid method is used to obtain an approximate solution for the decoupled pressure system in the first preconditioner stage. In the second stage, the classical ILU(0) preconditioner is applied to the fully implicit method system.

In this work, we demonstrate the accuracy and performance of the OBL approach to solve the problems with complex nonlinear physics by comparing DARTS modeling results with the legacy simulation. The paper is structured as follows. First, we briefly describe our numerical model and OBL approach. Next, we analyze the implementation and nonlinear behavior of capillarity operators. Then, several benchmark cases are performed in DARTS, followed by the comparison of accuracy and numerical performance against the reference solution based on the legacy simulation code. We end the paper with a discussion and main conclusions.

Methodology

Here, we briefly consider the governing equations and nonlinear formulations for multiphase multicomponent (e.g., dead oil with two phases and two components, and black oil with three phases and three components) isothermal simulations. The conservation of mass with n_p phases and n_c components is described by

$$\frac{\partial}{\partial t}\left(\phi \sum_{j=1}^{n_p} x_{cj}\rho_j s_j\right) + \operatorname{div}\sum_{j=1}^{n_p} x_{cj}\rho_j u_j + \sum_{j=1}^{n_p} x_{cj}\rho_j \tilde{q}_j = 0, \quad c = 1, 2, \ldots, n_c, \qquad (1)$$

where j is the corresponding phases (gas, water, and oil), ϕ is porosity, s_j is phase saturation, ρ_j is phase molar density, x_{cj} is component mole fraction in a phase, u_j is the velocity of each phase, and q_j is the volume flow rate of each phase caused by source and sink. In addition, Darcy's law is applied to describe the flow of each phase,

$$u_j = -K\frac{k_{rj}}{\mu_j}(\nabla p_j - \rho_j g \nabla D), \qquad (2)$$

where K is permeability tensor, k_{rj} is relative permeability, u_j is phase velocity, p_j is phase pressure, g is the gravitational acceleration, and D is the depth. For mathematical closure, one linear constraint and one nonlinear constraint are needed,

$$\sum_{j=1}^{n_p} s_j = 1, \qquad (3)$$

$$p_{c,ij} = p_i - p_j, \qquad (4)$$

where $p_{c,ij}$ is capillary pressure, which relates the pressures of the two phases, and p_i and p_j are pressures of the nonwetting and wetting phases, respectively. Capillary pressure is a function of saturation, often expressed as $p_{c,ij}(s_j)$. The capillary pressure/saturation relationship, also called the capillary pressure curve, can be measured in laboratories. In this work, the hysteresis in relative permeability and capillary pressure curves is neglected, whereby k_{rj} and $p_{c,ij}$ depend only on saturation.

A finite-volume discretization on a general structured mesh and backward-Euler approximation in time is applied,

$$V\left(\phi \sum_{j=1}^{n_p} x_{cj}\rho_j s_j\right)^{n+1} - \left(\phi \sum_{j=1}^{n_p} x_{cj}\rho_j s_j\right)^{n} - \Delta t \sum_{l}\sum_{j=1}^{n_p} x_{cj}^l \rho_j^l \Gamma_j^l \Psi^l + \Delta t \sum_{j=1}^{n_p} x_{cj}\rho_j q_j = 0, \qquad (5)$$

where $\Gamma_j^l = \Gamma^l k_{rj}^l / \mu_j^l$ is a phase j transmissibility over interface l, and Γ^l is the constant geometrical part of transmissibility. Ψ^l is the pressure difference at the interface. Eq. 1 is approximated in space using two-point flux approximation and in time using the fully implicit method. This introduces strong nonlinearity into the system of the governing equations. Next, we need to linearize the problem, which requires the determination of all the partial derivatives with respect to these nonlinear unknowns and assembling of the Jacobian matrix and residuals. After the linearization step using the Newton-Raphson method, the linearized system of equations is solved on each nonlinear iteration in the form

$$J(\omega^k)(\omega^{k+1} - \omega^k) = -r(\omega^k), \qquad (6)$$

where $J(\omega^k)$ and $r(\omega^k)$ are the Jacobian matrix and residual defined at the nonlinear iteration k, and ω is the primary unknown variable. In the conventional simulation, the Jacobian is assembled using accurate numerical property values and their derivatives with respect to nonlinear unknowns. This process often requires various interpolations (for properties such as relative permeabilities of different

phases) or a solution of a highly nonlinear system in combination with the chain rule and inverse theorem [for multiphase flash, see Voskov and Tchelepi (2012) for details] or their combination. In any case, the complexity of the simulation code and the corresponding computational cost increase.

OBL Approach

In this section, we present the OBL approach, which reduces the complexity of the simulation framework and helps to control the nonlinearity of complex physical problems, in the presence of buoyancy and capillarity in particular.

Transformation of Governing Equation. Following the OBL approach, all variables in Eq. 1 fully defined by the physical state ω can be grouped together and represented by the state-dependent operators (Khait and Voskov 2017; Voskov 2017). Taking into account buoyancy and capillarity, the discretized mass-conservation equation in operator form is

$$V\phi_0[\alpha_c(\omega)-\alpha_c(\omega_n)]+\sum_{l\in L(i)}\sum_{j}^{n_p}\Delta t\Gamma^l\Phi_j^l\beta_{cj}^l(\omega)+\theta(\xi,\omega,u)=0, \quad \ldots\ldots (7)$$

where

$$\alpha_c(\omega)=[1+c_r(p-p_{\mathrm{ref}})]\sum_{j=1}^{n_p}x_{cj}\rho_j s_j, \quad \ldots\ldots (8)$$

$$\beta_{cj}(\omega)=x_{cj}\rho_j k_{rj}/\mu_j, \quad \ldots\ldots (9)$$

$$\theta(\xi,\omega,u)=\Delta t\sum_{j=1}^{n_p}x_{cj}\rho_j q_j(\xi,\omega,u), \quad \ldots\ldots (10)$$

where ω and ω_n are nonlinear unknowns on the current and previous timestep, respectively; $L(i)$ is the set of neighbors of the control volume l; and $\theta(\xi,\omega,u)$ is the source term. V, ϕ_0, and c_r are initial volume, porosity, and rock compressibility, respectively, which represent the reservoir-rock properties, and ρ_j, k_{rj}, and μ_j, are phase density, phase relative permeability, and phase viscosity, respectively, Γ^l is a constant geometrical part of transmissibility, Φ_j^l is the phase-potential difference at the interface. Here, the PPU strategy is applied to compute the numerical flux in DARTS. The phase j potential difference between blocks 1 and 2 (assuming only one capillary pressure between two phases) can be written as

$$\Phi_{j,12}=p_1-p_{c,1}-(p_2-p_{c,2})-\frac{\rho_j(\omega_1)+\rho_j(\omega_2)}{2}g(D_2-D_1). \quad \ldots\ldots (11)$$

In this work, gravity and capillary pressure terms are treated as two standalone operators that depend only on the physical state. For the gravity operator, we followed the idea proposed in Khait and Voskov (2018a), where n_p mass-density operators (ρ_j) are being introduced for each phase. Besides, n_p capillary pressure operators are introduced to this system. For an n_p-phase system, only n_p-1 capillary pressures are needed for the calculation of phase pressure. Here, the capillary pressure operator of the reference phase is defined as zero to keep the whole system coordinated.

In this study, the Brooks and Corey (1964) – type model is applied for the calculation of capillary pressure operators. A straightforward implementation of PPU within the OBL approach implies the increase in the number of flux operators from n_c to $n_c n_p$, because each phase should be treated separately. Hence, OBL with PPU requires $n_c+n_c n_p+n_p+n_p$ operators for the isothermal problem with n_c components and n_p phases (excluding the accumulation operators),

$$\beta_{cj}(\omega)=x_{cj,12}\rho_{j,12}k_{rj,12}/\mu_{j,12}=\begin{cases}x_{cj,1}\rho_{j,1}k_{rj,1}/\mu_{j,1} & \text{if} \quad \Phi_{j,12}>0\\ x_{cj,2}\rho_{j,2}k_{rj,2}/\mu_{j,2} & \text{otherwise,}\end{cases} \quad \ldots\ldots (12)$$

$$\delta_j(\omega)=\rho_j g, \quad \ldots\ldots (13)$$

$$\zeta_j(\omega)=p_{c,j}, \quad \ldots\ldots (14)$$

where δ_j and ζ_j are gravity and capillarity operators, respectively, only dependent on physical state.

This representation allows us to simplify the complicated nonlinear physics and implementation of the generic linearization approach. Instead of performing complex evaluations of properties and their derivatives with respect to nonlinear unknowns during the simulation, we can parameterize operators in physical space at the preprocessing stage or adaptively (Khait and Voskov 2018a). The parameter space depends on the investigated physical problem. In a dead-oil isothermal kernel, for instance, the nonlinear unknown variables are pressure p and water composition z_w. If the OBL resolution is set as 100, a 2D parameter space with 100×100 supporting points is constructed and the interpolation is executed in this 2D space. Then, during the simulation, a bilinear interpolation is applied to evaluate the operators in the current timestep **(Fig. 1),** which improves the performance of the linearization stage. Meanwhile, this approach can reduce the nonlinearity of the physical problem because of the application of a piecewise linear representation of operators (Khait and Voskov 2018b).

Nonlinear Capillarity Operator. Gravity operators include mass density for each phase and are monotonically dependent on the pressure. The derivatives of gravity operators with respect to the unknowns do not change significantly and are related to the fluid compressibility. However, the relationships between capillary pressure and saturation (composition) are more complicated and highly nonlinear.

To examine the nonlinearity of this operator, we show an example of a water/oil system with a Corey-type capillary pressure curve,

$$p_c(\omega)=p_d\left(\frac{S_w(\omega)-S_{wc}}{1-S_{wc}-S_{or}}\right)^{-1/\lambda}, \quad \ldots\ldots (15)$$

$$\frac{\partial p_c}{\partial \omega} = \frac{\partial p_c}{\partial S_w}\frac{\partial S_w}{\partial \omega}, \quad (16)$$

where p_d is the capillary entry pressure, which we take as 0.2 bar. S_{wc} and S_{or} are the connate water saturation (0.12) and residual oil saturation (0.16), respectively. Both Eqs. 15 and 16 are highly nonlinear equations.

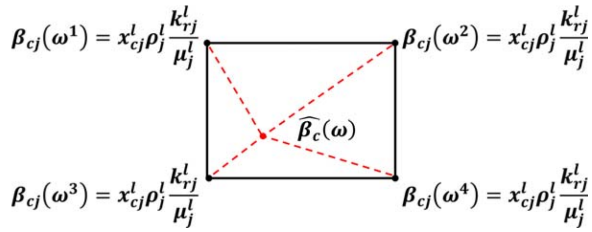

Fig. 1—Schematic of interpolation process for β operators. ω^1 through ω^4 are four supporting points, and ω is the current physical state of a given control volume at a given timestep in the simulation.

Capillary pressure depends only on saturation in the two-phase system if hysteresis effects are not present. Typically, a capillary pressure table, giving the relationship between saturation and capillary pressure, should be provided to interpolate the p_c value depending on the saturation. In the course of the simulation, the derivative of capillary pressure with respect to the physical unknowns needs to be assembled in the Jacobian. Here, we investigate the behavior of the capillary operator with the processed table.

As shown in **Fig. 2a,** instead of plotting capillary pressure (p_c) vs. water saturation (S_w), we plot the relationship between p_c and water composition (z_w) because our primary unknown variables are pressure and the overall composition of each component. With increasing water composition, capillary pressure decreases (behavior similar to p_c vs. S_w). Note that the relationship between p_c and z_w is not piecewise-linear despite the relationship between p_c and S_w being so. This happens as a result of the different phase densities, because the conversions of composition and saturation rely on phase densities as well. The shape of the capillary pressure curve is distinct with different lengths of the given table, and a finer table gives a smoother curve. A similar difference between derivatives can be found in Fig. 2b. The derivatives of capillary pressure with respect to water composition exhibit discontinuity in both cases. In turn, the large discontinuity can cause numerical issues, such as in the Newton convergence, and especially in capillary-dominated flow. With a finer resolution in the table, this issue can be moderated, thus improving the numerical performance.

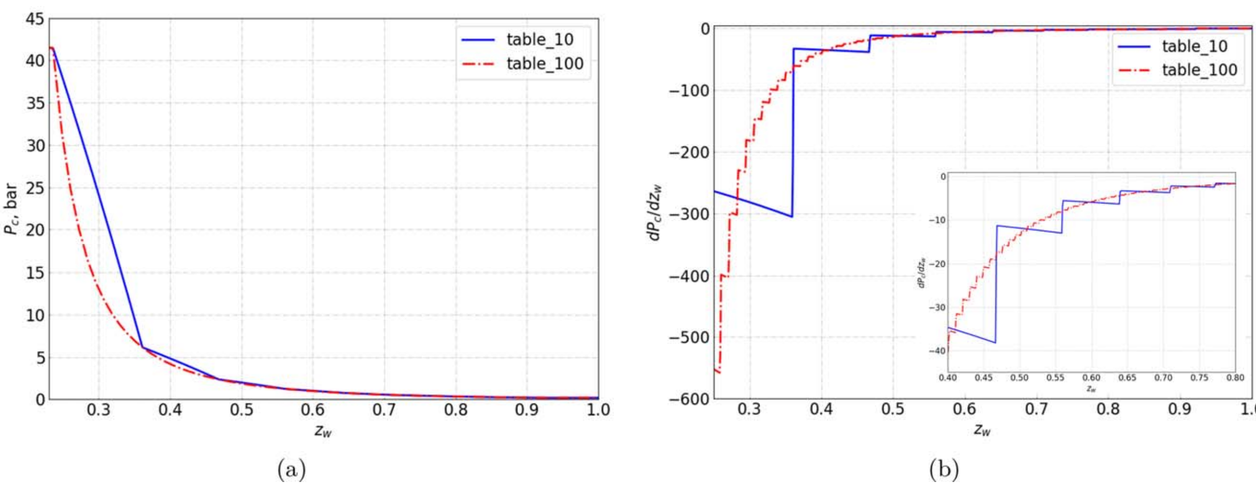

Fig. 2—(a) Capillary pressure and (b) its derivative with respect to composition; table_10 and table_100 represent 10 and 100 supporting points in the given table, respectively. The inset zooms in (b) locally for a better visualization.

To avoid numerical issues, one either can provide a table containing more points to interpolate p_c or implement the analytical model to evaluate p_c and corresponding derivatives. In DARTS, both approaches are applied. First, an analytical capillary pressure model is defined. Then, by increasing the OBL resolution (e.g., $n = 100$, meaning a p_c table with 100 supporting points for a capillary state-dependent operator), we improve the accuracy of a simulation.

Numerical Results

In this section, we compare the numerical results between DARTS and a legacy reservoir simulator that uses the conventional linearization approach. A 1D black-oil segregation model validates our approach. Then, four benchmark cases are selected to test the accuracy and efficiency of our new simulator: the extended first SPE Comparative Study (Odeh 1981), the ninth SPE Comparative Study (Killough 1995), the 10th SPE Comparative Study (dead-oil) (Christie and Blunt 2001), a synthetic UNISIM-I model (Gaspar et al. 2015), and the 10th SPE Comparative Study (compositional). The corresponding introduction of each case is briefly described at the beginning of each comparison section, which is followed by the performance of both simulators. To make the results comparable, the convergence parameters (such as maximum iterations and tolerances for both linear and nonlinear solvers) and timestep selection are made similar for both simulators, while the other parameters are kept as default. Because of the absence of detailed information regarding CPU time of Jacobian assembly in the legacy simulator output, we will only compare the resulting time and corresponding computational characteristics.

1D Homogeneous Vertical Reservoir. Here, we build a conceptual vertical 1D reservoir of 1000-m depth under buoyancy- and capillarity-driven flow with black-oil physics. Porosity and permeability are set as constants of 0.2 and 100 md, respectively. Finite-volume discretization on a standard Cartesian grid with block sizes $\Delta x = 10$ m, $\Delta y = 10$ m, and $\Delta z = 10$ m are applied to discretize the domain. Only gas can dissolve in the oil phase in the black-oil formulation, and most of the properties described here are derived from a table correlation. Initially, the top five grid cells are filled with water (higher density), whereas the bottom five cells are filled with oil (lower density). All phases are compressible. The reservoir is initialized with linearly increasing pressure (the pressure of first cell $P_0 =$ 260 bar, and the increment is 10 bar/cell), and the bubblepoint pressure P_b is set to 270 bar. All simulations are run for 10,000 days until the system reaches an equilibrium state. Stone I relative permeability and the Brooks and Corey (1964) capillary model are used to interpolate the fluid properties.

Figs. 3 and 4 show the dynamic distribution of fluids in the absence and presence of capillarity. It can be seen that without capillarity, the heavier water phase, initially placed on the top, exchanges positions with the oil phase by the end of the simulation time (Fig. 3). However, in the presence of capillarity, water and oil cannot segregate completely; instead, there is a transition zone forming above the bottomwater-saturated cells (Fig. 4). In this segregation process, with decreasing water saturation, the corresponding capillary pressure between oil and water phase increases. Once the gravity force cannot overcome the capillary force, the water phase is then locked there as a remaining phase. Compared with gravity segregation without the capillary force, capillary pressure causes a lower oil saturation in the upper cells, while a higher oil saturation in the lower cells (i.e., the capillary pressure) hinders the oil phase moving upward. In both cases, a small amount of gas is released from the oil phase and accumulates on the top cell, leading to a lower oil saturation there.

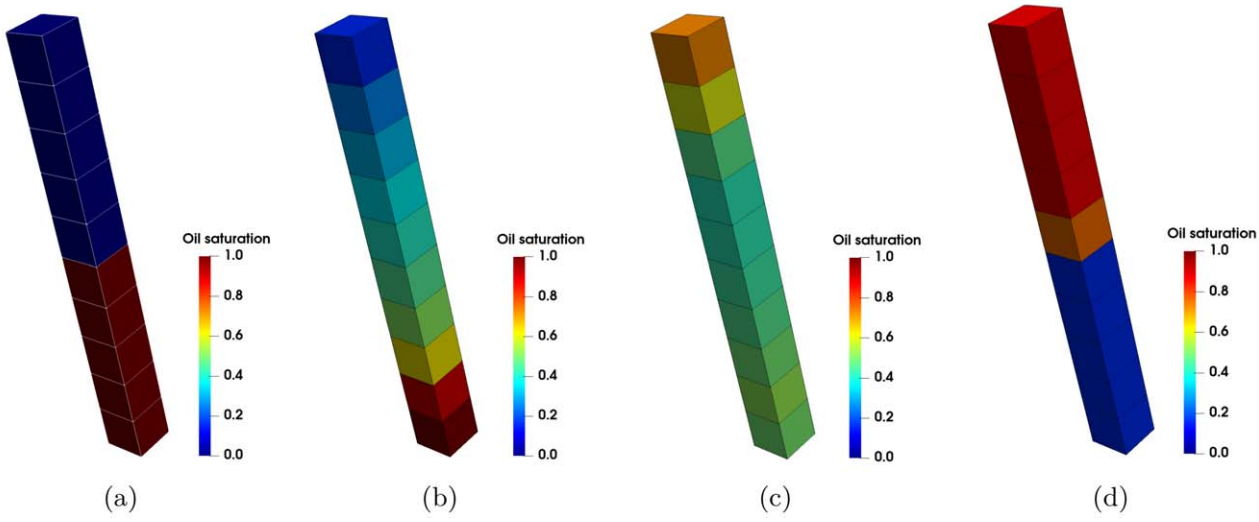

Fig. 3—Black-oil gravity segregation: (a) initial condition; (b) 500 days; (c) 1,000 days; (d) 10,000 days.

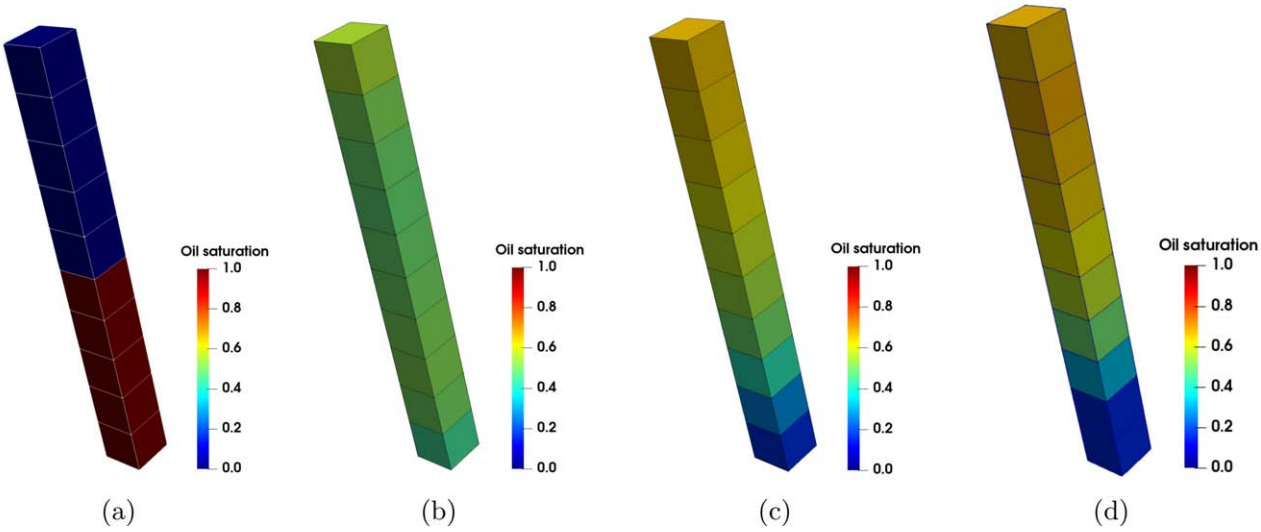

Fig. 4—Black-oil gravity segregation with capillarity: (a) initial condition; (b) 500 days; (c) 1,000 days; (d) 10,000 days.

Table 1 presents the simulation results obtained using different OBL resolutions. The number of points in the first column represents the OBL resolution in the parameter space. The second column indicates the total number of nonlinear iterations by the end of the simulation. The third, fourth, and fifth columns correspond to the maximum differences in pressure, water-saturation, and oil-saturation solutions, respectively, compared with the results obtained by the legacy simulator. It can be seen from Table 1 that with a coarse OBL

resolution, there is a big difference between the solutions with conventional linearization of nonlinear physics vs. the parametrized solutions, especially for pressure. However, if the OBL resolution increases, the difference decreases significantly, corresponding with a minor increase in the nonlinear iterations. This is because as parametrization in physics is refined, the shape of state-dependent operators becomes more nonlinear, causing the increase in nonlinear iterations. At the same time, the number of nonlinear iterations for 500 and 1,000 points is nearly the same, while the discrepancy of pressure and saturation solutions is significantly reduced. This reflects the fact that the location of points in the current OBL approach is chosen blindly, depending on a uniform distribution without any analysis of nonlinearity (Khait and Voskov 2018a). The comparison of CPU time shows that the computational cost is reduced significantly by using the OBL approach, compared with the conventional simulation. As a result, DARTS exhibits both high accuracy and robustness.

Resolutions	Newton Iterations	E_p	E_{sw}	E_{so}	CPU Time (seconds)
Legacy Simulator	1,198	–	–	–	5.5
$n = 100$	1,196	42.0	0.007	0.035	0.192
$n = 500$	1,227	6.9	0.007	0.024	0.297
$n = 1{,}000$	1,230	2.38	0.002	0.015	0.324

Table 1—Numerical difference and nonlinear behavior of 1D black-oil simulation.

First SPE Comparative Study. This is a basic test for a three-phase three-component black-oil modeling technique using gasflooding. The top of the reservoir is at 2540 m, with a total thickness of 30 m. The corresponding pressure/volume/temperature properties, relative permeabilities, and reservoir conditions can be found in Odeh (1981). The difference with the original model is that in this case the capillary effect is included, which increases the nonlinearity of the problem. There are two vertical wells located in the opposite corners of the domain: gas is injected from the top layer with fixed bottomhole pressure (BHP; 400 bar), whereas oil is produced from the bottom layer by controlling the oil-production rate (3000 m^3/d). The Stone I relative permeability model and the Brooks and Corey (1964) capillary pressure model are used to interpolate the fluid properties. In the water/oil system, p_d is 0.2 bar and the exponent λ is 0.5, whereas in the gas/oil system, p_d is 0.12 bar and the exponent λ is 0.8. Then we can obtain the corresponding capillary pressure curves using Eq. 15. All simulations are run for 10 years with a maximum timestep of $\Delta t = 10$ days. There is no gas in the initial condition. The large density difference between liquid and gas leads to small changes in gas composition (i.e., higher OBL resolution is required to interpolate gas properties). To reduce the OBL performance and maintain accuracy, we take the logarithmic axes for composition space instead of using uniform parametrization space in this case, with an OBL resolution of 1,000.

Fig. 5 shows the comparison of well rates and BHPs of a producer between two simulators. Before the gas breakthrough, the oil-production rate keeps constant with a certain gas/oil ratio. Once the injected gas arrives at the producer, the oil-production rate decreases quickly; the gas-production rate, however, increases significantly, leading to a lower BHP at the producer. Under the chosen OBL resolution, DARTS demonstrates a good match with the solution of the legacy simulator.

Fig. 6 shows the results by the end of the simulation. Gas is injected from the top layer, leading to a relatively higher gas saturation and lower oil saturation on the top layer (Figs. 6b and 6c). To show the solution difference of each layer between DARTS and the legacy simulator, the l_2 norm is adopted to evaluate the relative difference in each layer. The normalized difference of the kth layer can be calculated as

$$e^k = \frac{||\vec{x_1}^k - \vec{x_2}^k||_2}{||\vec{x_2}^k||_2}. \quad (17)$$

The relative differences of pressure and water saturation are plotted in **Fig. 7a.** As is shown, the relative difference of each layer is fairly small (pressure difference is less than 2.0%, and maximum gas saturation difference is less than 3.5%) under this OBL resolution, which exhibits a good match between two very different simulation software.

Fig. 7b displays the performance of DARTS and the legacy simulator in terms of nonlinear iterations, linear iterations, and CPU time. The number of nonlinear iteration of DARTS is slightly reduced (790 vs. 803), but DARTS requires more linear iterations compared with the legacy simulator (3,164 vs. 2,116). However, because of the implementation of the OBL approach, the computational cost is in turn reduced significantly, approximately three times faster than the legacy simulator (1.25 seconds vs. 3.42 seconds). To improve the simulation performance by another order of magnitude further, one can run DARTS at GPU architecture (Khait et al. 2020).

Ninth SPE Comparative Study. Here, we present the ninth SPE comparative project, which is dependent on $24 \times 25 \times 15$ gridblocks placed on a dipping, initially undersaturated reservoir (dipping angle of 15° in the x-direction). The top of the reservoir is at 2743.2 m and the total thickness is 109.422 m, with variations in each layer. The gridblock is in conventional rectangular coordinates without local grid refinement. The reservoir has a high degree of heterogeneity provided by a geostatistically based permeability field, as shown in **Fig. 8a.** The permeability varies within the layers, whereas the porosity and thickness are homogeneous in every layer. There are 25 producers and a single water injector. All wells are operated under a constant rate. The water injector is set to a maximum rate of 795 m^3/d, with a maximum BHP of 300 bar. The maximum oil rate for all producers is set at 240 m^3/d in the beginning; at 300 days, the rate is switched to 15.9 m^3/d for all wells. Finally, at 360 days, the rate is again raised to 240 m^3/d for all producers until the end of the simulation at 900 days. The minimum BHP for all producers is set to 70 bar. Taking the great heterogeneity of the reservoir and complex physics into account, we directly use a higher OBL resolution with 1,000 supporting points in the logarithmic space.

One interesting feature of the water/oil capillary pressure curve, as shown in Fig. 8b, is the discontinuity around $S_w = 0.35$. After this saturation, the capillary pressure becomes negative. Such a discontinuity usually causes difficulties in Newton-Raphson convergence for cases in which water saturations are changing significantly. Another feature of the capillary pressure curve is the tail, which does not extend to a water saturation of unity. This feature does represent reality in certain reservoirs where imbibition might have occurred because of tectonics before discovery (Killough 1995). The main purpose of this test case is to investigate the complications brought by a high degree of heterogeneity in the permeability field and the highly nonlinear capillary pressure curve.

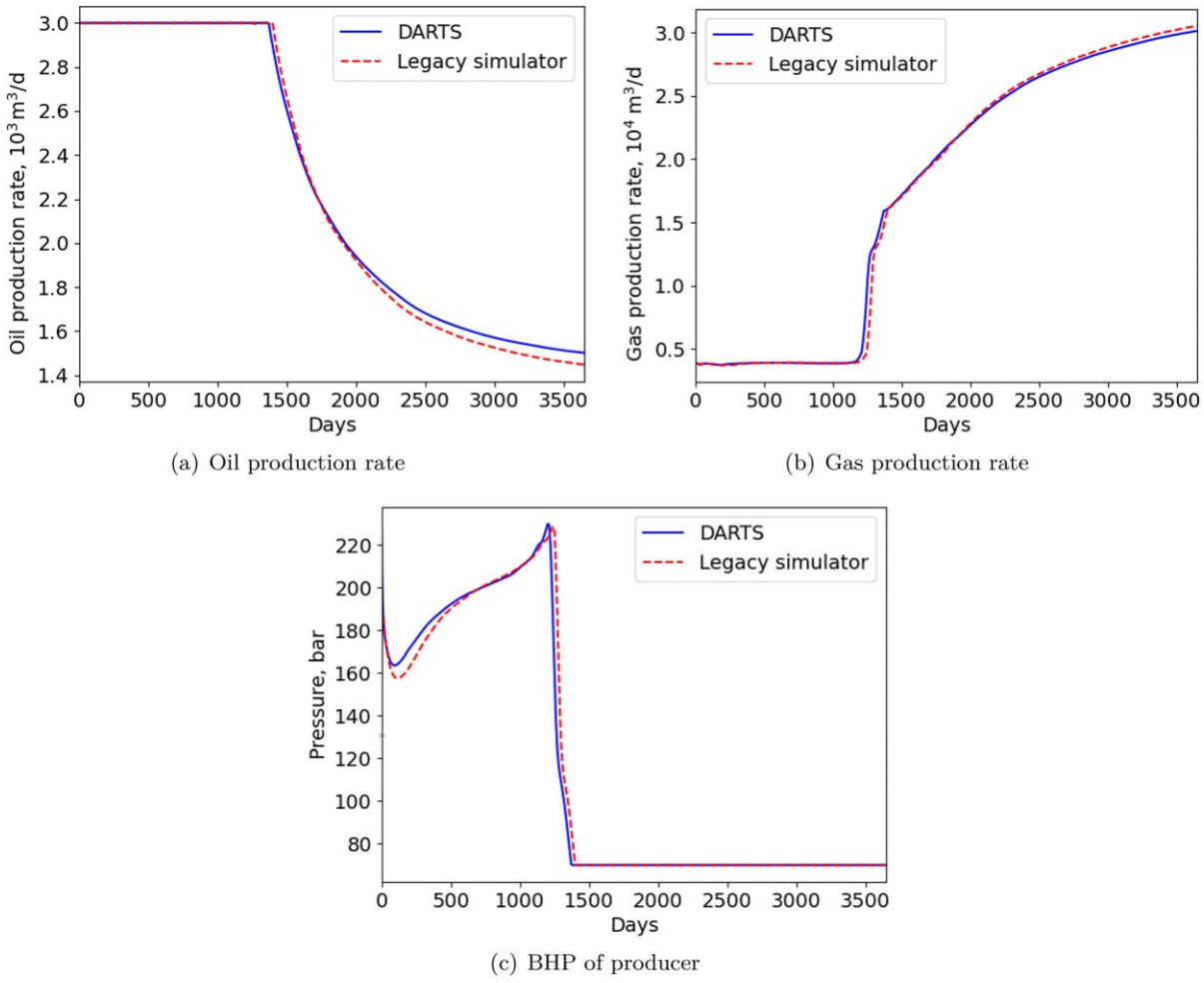

Fig. 5—Comparison of well rates and BHPs of producer with different simulators. All rates are calculated at surface conditions.

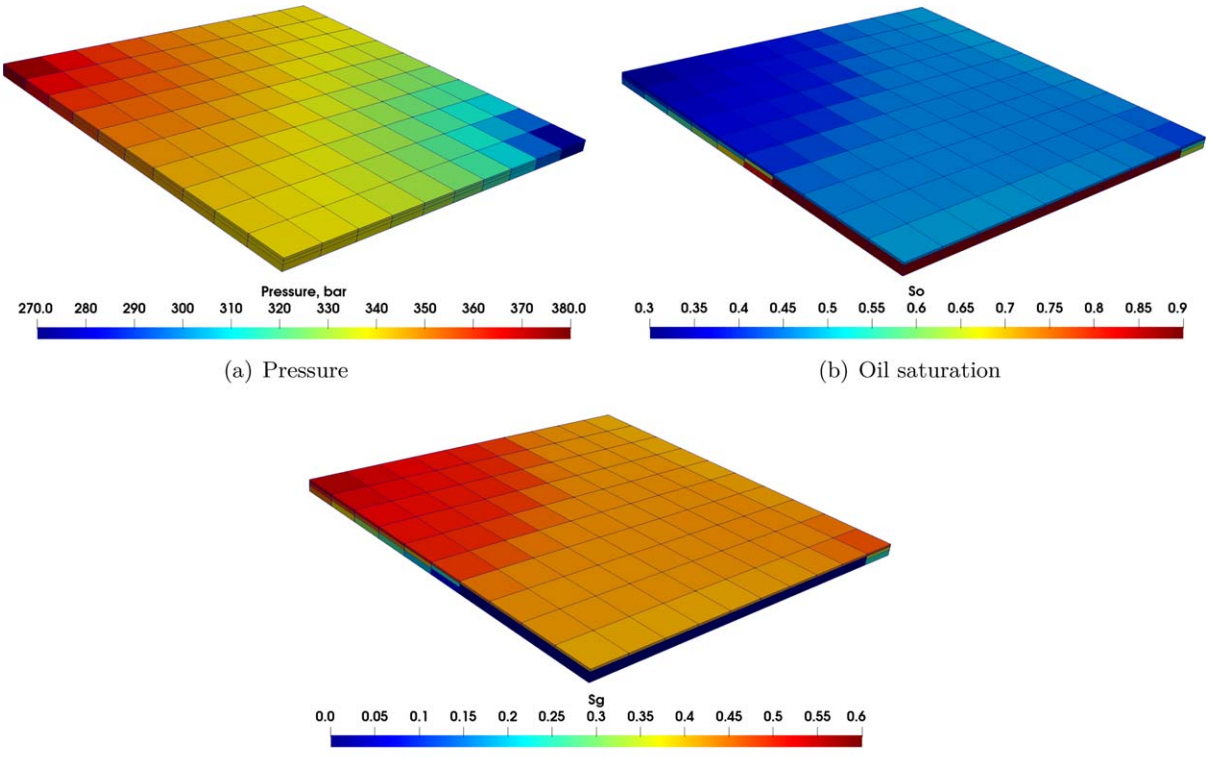

Fig. 6—Pressure and saturation profiles at $t = 10$ years.

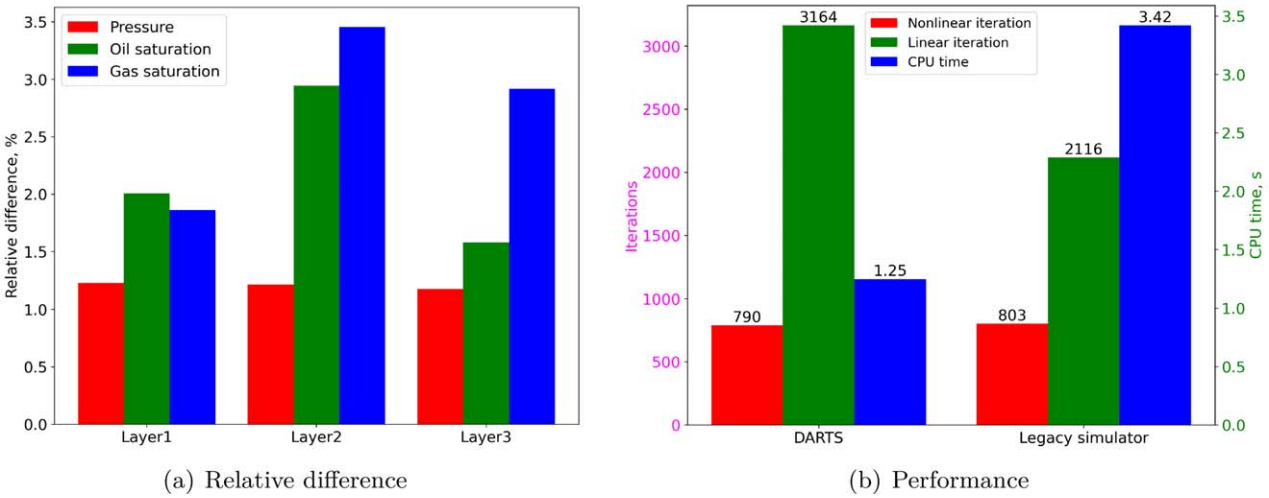

Fig. 7—Accuracy and performance of two simulators for the First SPE comparative study model. (a) Relative difference of pressure and saturation between DARTS and the legacy simulator in each layer. (b) Comparison of the numerical performance between two simulators.

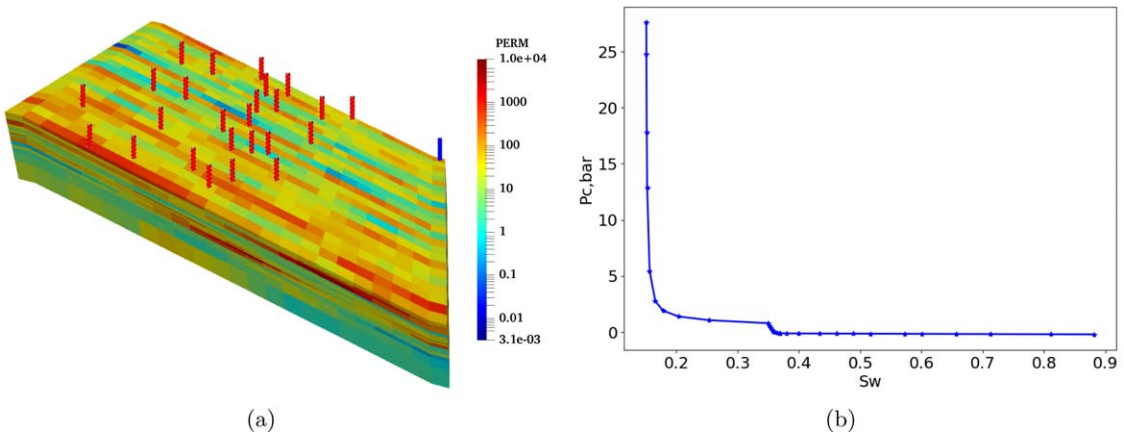

Fig. 8—(a) Permeability distribution and (b) water/oil capillary pressure curve in the Ninth SPE comparative project.

Fig. 9 displays the instantaneous well rates for the injector and all producers. The difference between the two simulations is negligible. In the gas-production rate (Fig. 9b), there are more pronounced differences in the first 40 days, which we again address by a slightly different well implementation. Saturation and pressure maps by the end of simulations are shown in **Fig. 10.** With water injection, oil is displaced to the producers located at the top of the domain, resulting in a lower oil saturation near the water-saturated region. The pressure is also lower on the top of the domain. Once it is less than bubblepoint pressure, gas evaporates from oil and accumulates in the upper part of the reservoir, leading to higher gas saturation there. **Fig. 11a** illustrates the relative difference of each layer between DARTS and the reference (l_2 norm). The differences of pressure and saturations are approximately 2.0%. These results indicate the capacity of the OBL approach to accurately model complex physical problems with convection, buoyancy, and capillarity.

Fig. 11b shows the numerical performance of DARTS and the legacy simulator. It can be seen that DARTS takes fewer nonlinear iterations compared with the legacy simulator (379 vs. 438), although the number of linear iterations of DARTS is still higher (3,689 vs. 1,064). In terms of computational time (12.50 vs. 19.17 seconds), DARTS is more efficient, although the performance gain is not very significant.

UNISIM-I Synthetic Model. The UNISIM-I model is a synthetic model using publicly available data from Namorado Field, Campos Basin, Brazil. This model is designed for uncertainty reduction (Avansi and Schiozer 2015). There are four conditioning vertical wells to obtain the initial porosity distribution by petrophysical modeling **(Fig. 12a),** and one porosity/permeability correlation is used to interpolate the permeability distribution (Fig. 12b). This reservoir is highly heterogeneous, with several faults. The domain is discretized into a corner-point grid with $81 \times 58 \times 15$ cells (28,676 active cells). This project contains 14 production wells and 11 injection wells. The maximum oil rate for all producers is set at 800 m^3/d with a maximum BHP of 35.3 bar, and all injectors are controlled by a water-injection rate of 1200 m^3/d. Other reservoir parameters are described in Gaspar et al. (2015). The simulation time spans 10 years with a maximum timestep of 15 days. In the original model, the capillary pressure between the gas and oil phases is ignored. Therefore, we consider only the capillary pressure between oil and water phases. An OBL resolution with 1,000 supporting points in logarithmic space is used in this case as well.

Fig. 13 displays the total well rates for all producers. There is a small deviation from the reference solution, but in general, the match is acceptable. Pressure and oil-saturation profiles between the two simulators are shown in **Fig. 14.** The relative difference of each layer (Eq. 17) in terms of pressure and saturation is displayed in **Fig. 15a.** In this case, by the end of the simulation, the differences between the results of the two simulations vary insignificantly.

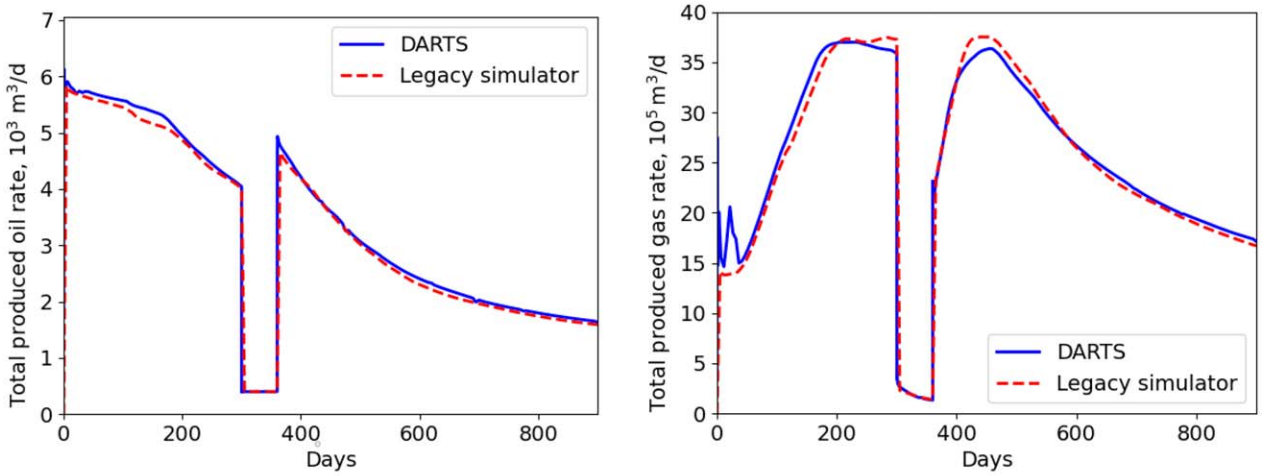

(a) Oil production rate

(b) Gas production rate

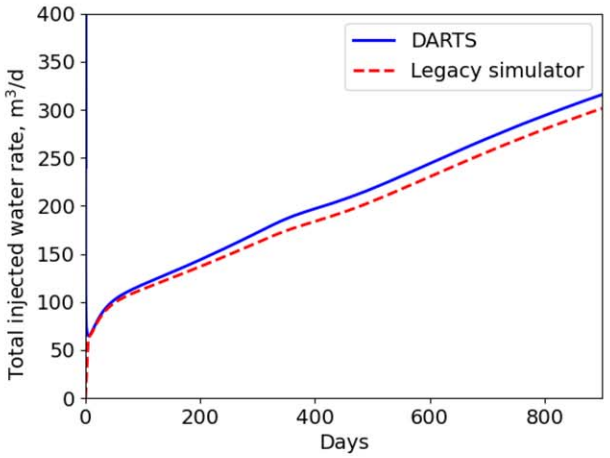

(c) Water injection rate

Fig. 9—Comparison of total well rates between DARTS and reference. All rates are calculated at surface conditions.

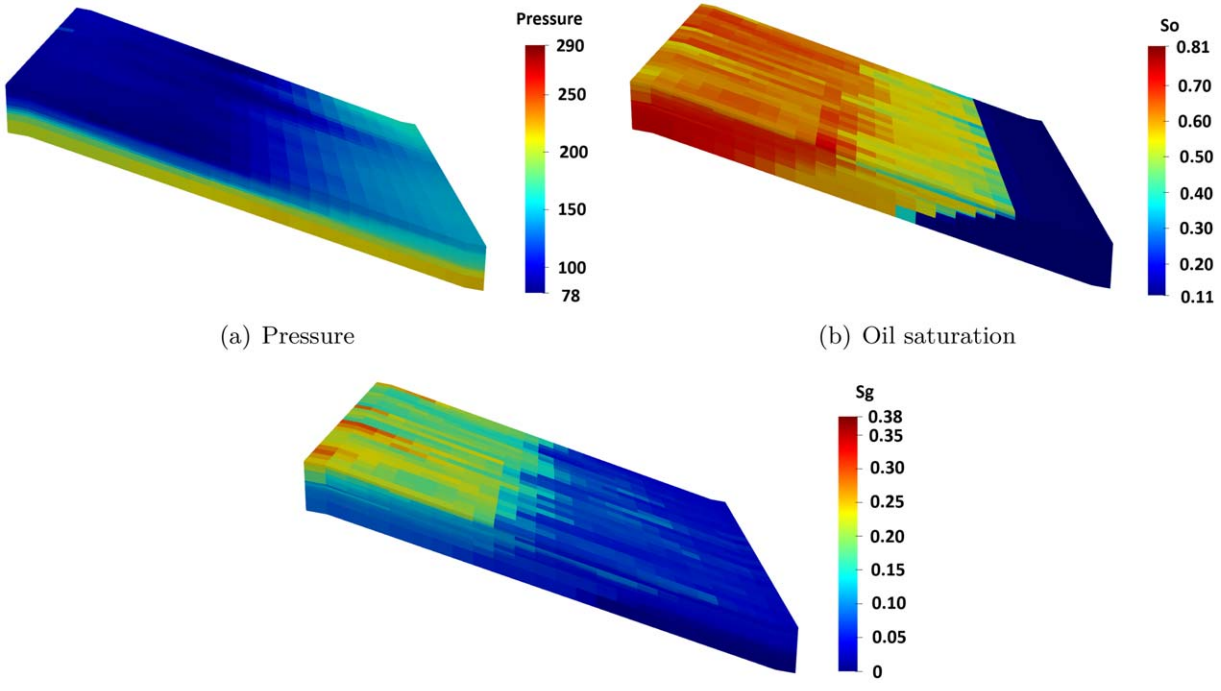

(a) Pressure

(b) Oil saturation

(c) Gas saturation

Fig. 10—Simulation results of pressure and saturations at the end of simulation.

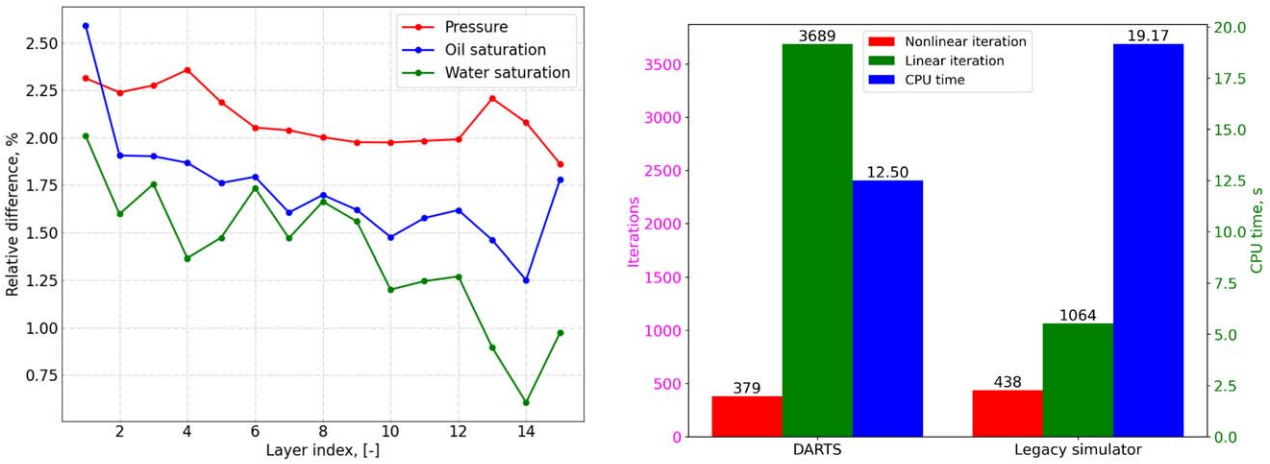

(a) Relative difference (b) Performance

Fig. 11—Accuracy and performance of two simulators for the 9th SPE comparative study model. (a) Relative difference of pressure and saturation between DARTS and the legacy simulator in each layer. (b) Comparison of the numerical performance between two simulators.

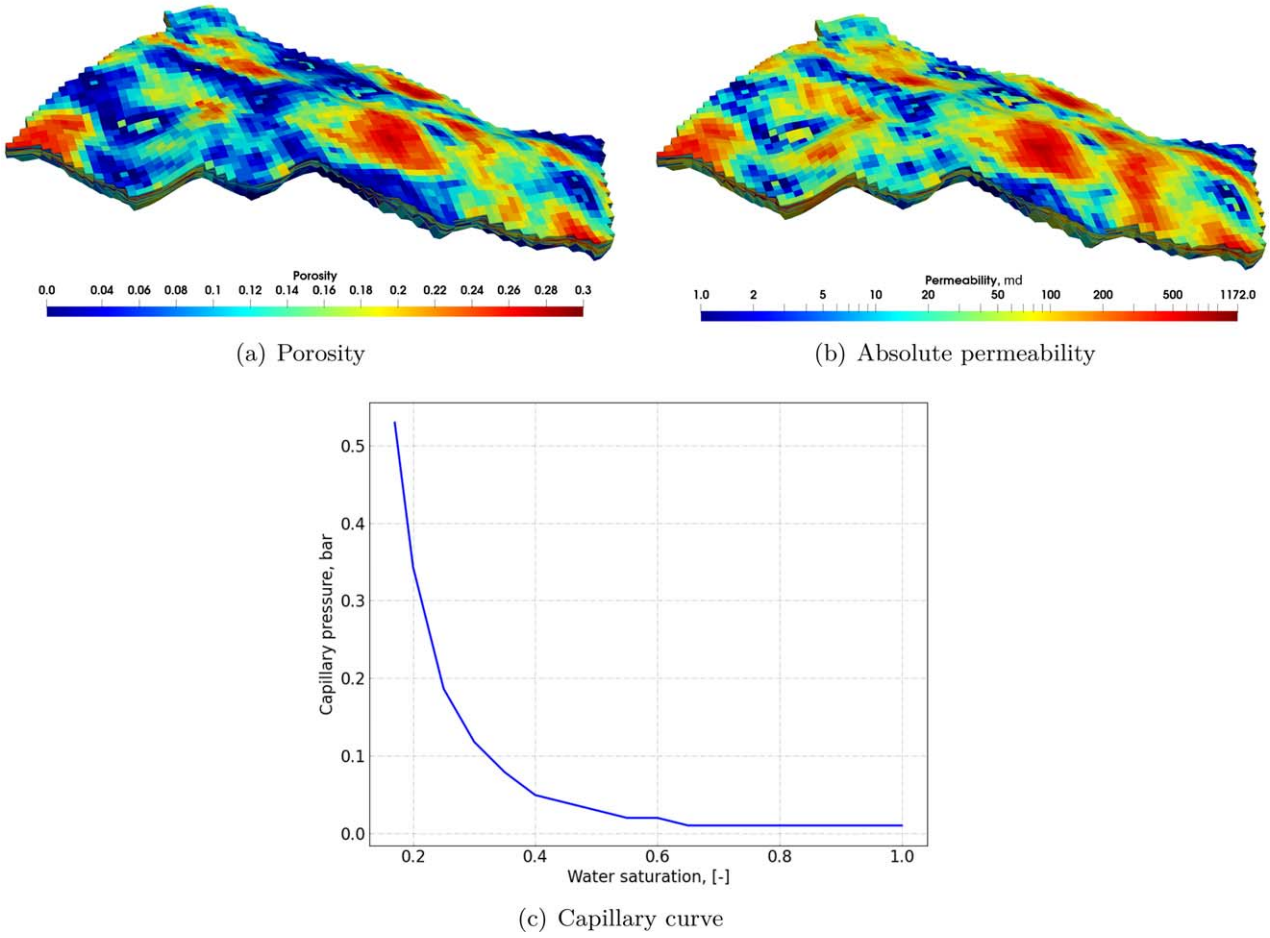

(a) Porosity (b) Absolute permeability

(c) Capillary curve

Fig. 12—Porosity and permeability distribution, and capillary pressure curve of UNISIM-I model.

Fig. 15b shows the performance of two simulators by the end of the modeling period. DARTS requires fewer Newton iterations by using the OBL approach. As in the previous cases, DARTS needs more linear iterations to converge (2,064 vs. 1,081), while the computational performance of DARTS is better (56.0 vs. 142.95 seconds).

10th SPE Comparative Study. This is another benchmark problem involving oil production from a severely heterogeneous reservoir using a waterflooding technique. The top of the reservoir is at 3657.6 m and the total thickness is 51.8 m. Because the full model challenges the linear solver of the legacy simulator too much, we only extract the seventh layer of shallow-marine Tarbert Formation (corresponding thickness is 0.6096 m). The formation, which is characterized by large permeability variations **(Fig. 16a),** is defined on a

regular Cartesian grid with $60 \times 220 \times 1$ (13,200) cells. The porosity field (Fig. 16b) is strongly correlated with the permeability. We add a capillary pressure curve (Fig. 16c), using the Brooks and Corey (1964) model ($p_d = 0.15$ bar and $\lambda = 0.8$). There are four producers (at four corners) operated under constant BHP (150 bar) and one water injector (in the center) with a constant injection rate (5 m^3/d). A five-spot layout is used for the well locations. In this case, the OBL resolution is set to 1000 points. All simulations are run for 1,000 days with a maximum timestep of $\Delta t = 10$ days because the legacy simulator in the default mode has a convergence issue with larger timesteps. The other parameters, such as relative permeability and the pressure/volume/temperature table, can be found in Christie and Blunt (2001).

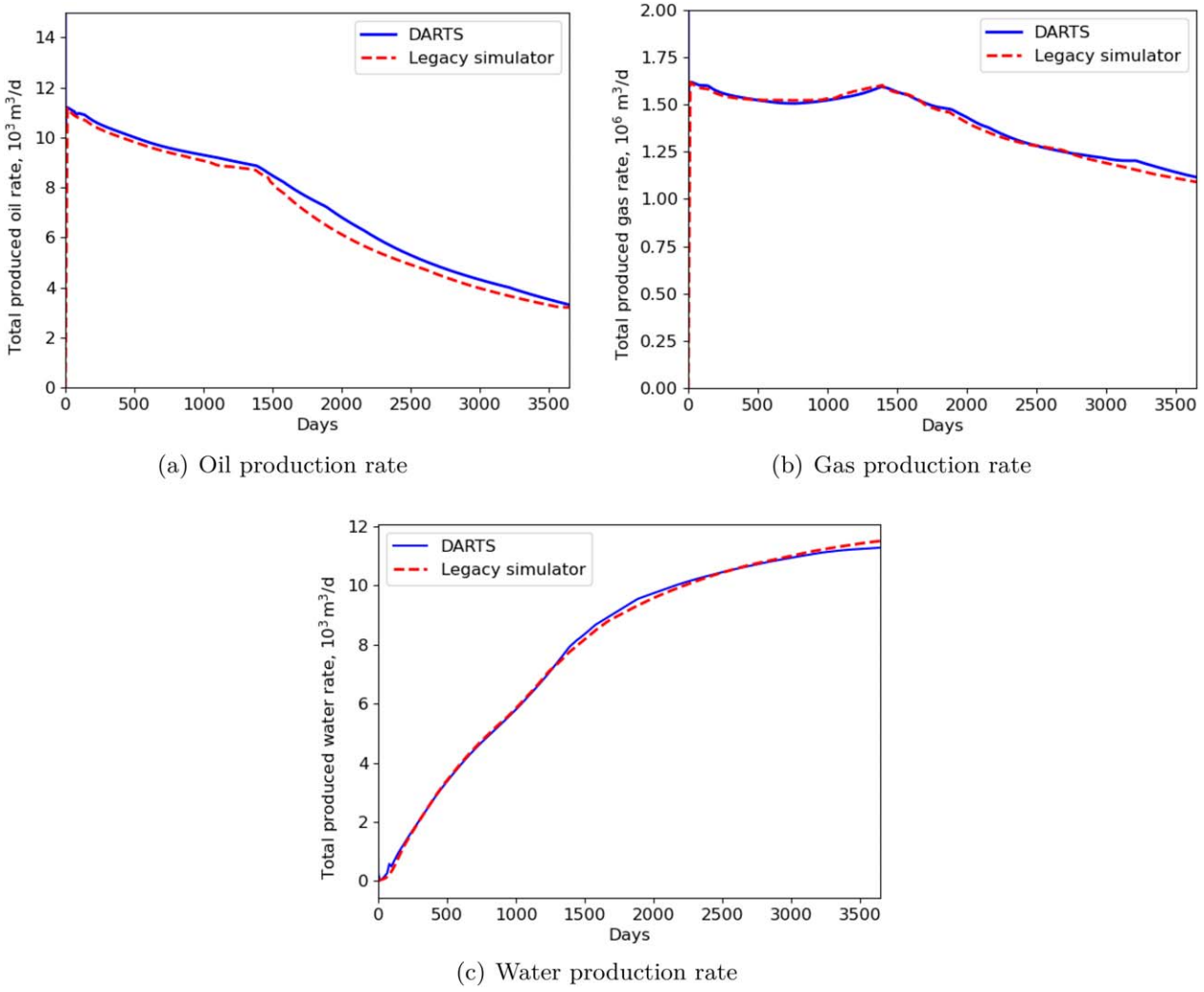

Fig. 13—Comparison of total well rates between DARTS and the legacy simulator. All rates are calculated at surface conditions.

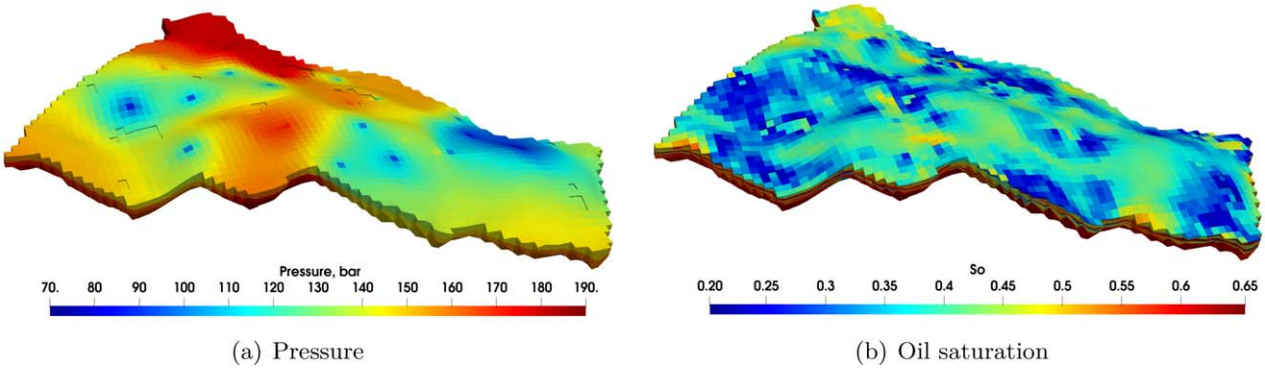

Fig. 14—Comparison of pressure and oil-saturation distribution between DARTS and the legacy simulator.

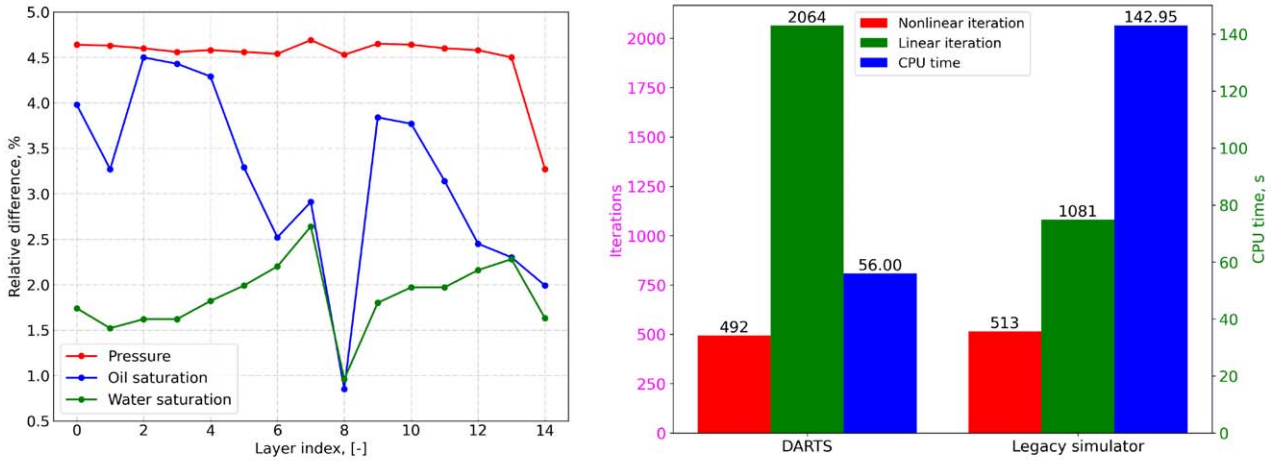

(a) Relative difference (b) Performance

Fig. 15—Accuracy and performance of two simulators for UNISIM model. (a) Relative difference of pressure and saturation between DARTS and the legacy simulator in each layer. (b) Comparison of the numerical performance between two simulators.

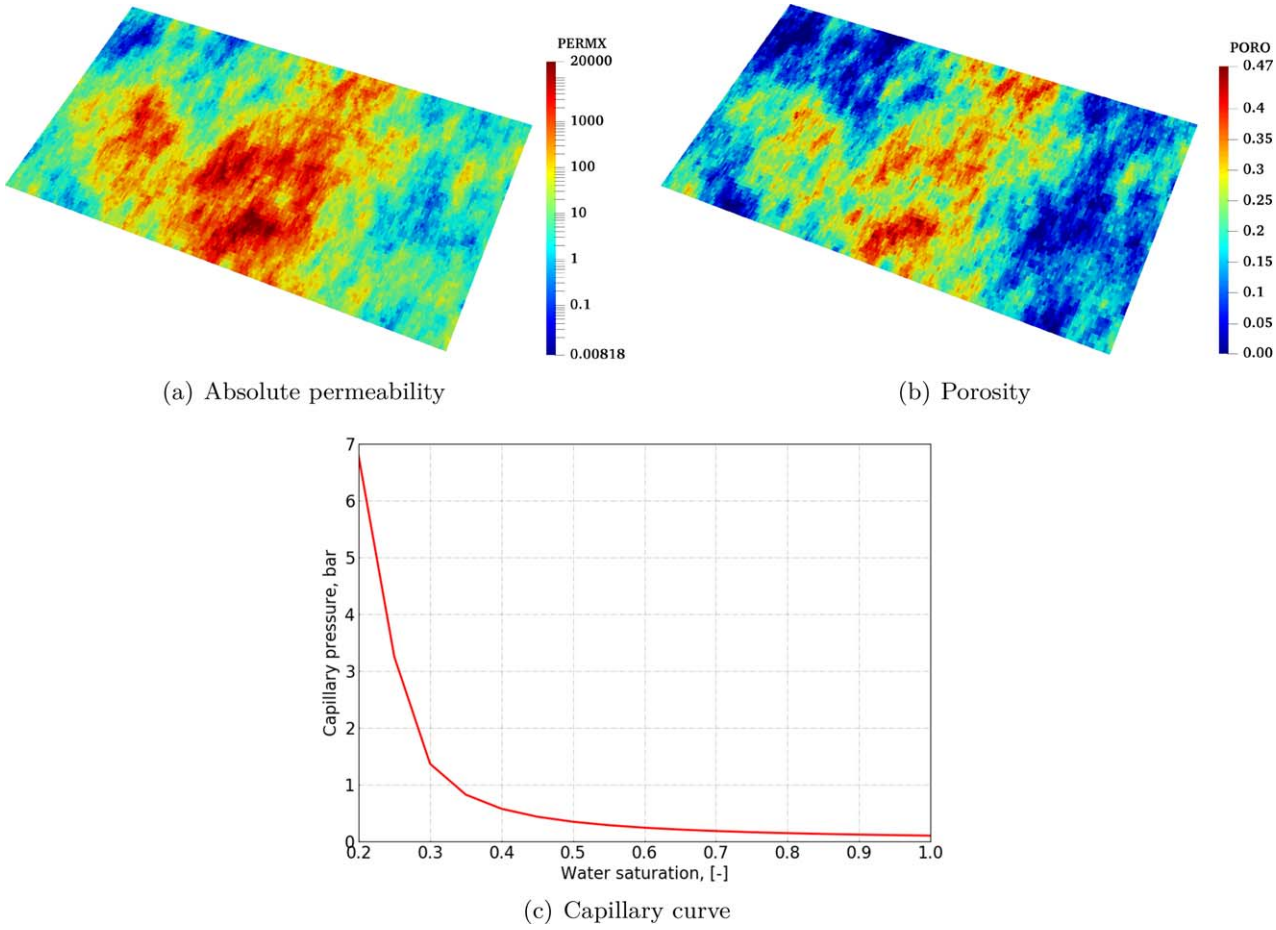

(a) Absolute permeability (b) Porosity

(c) Capillary curve

Fig. 16—Porosity and permeability distribution, and capillary pressure curve of the 10th SPE comparative study model.

Fig. 17 shows the changes in total oil-production rate, total water-production rate, and BHP of the injector. Before water breakthrough, only oil is produced, and its rate increases with time. After the water breaks through to the producers, the total oil-production rate starts to decrease because of the higher relative mobility of the water phase. In the presence of highly nonlinear convective flow, gravity, and capillarity, DARTS shows a perfect match with the legacy simulator. Because of the high level of heterogeneity, the saturation of the domain varies over a large range **(Fig. 18c).** Water can easily displace the oil in the high-permeability zone, leading to relatively low oil saturation. However, oil is difficult to move in the low-permeability region. The relative differences of pressure and water saturation in this layer are plotted in Figs. 18b and 18d. As is shown, the relative difference is reasonably small (pressure less than 1.0% and saturation less than 3.0%) under the chosen OBL resolution, which again exhibits a good match between two very different simulation codes.

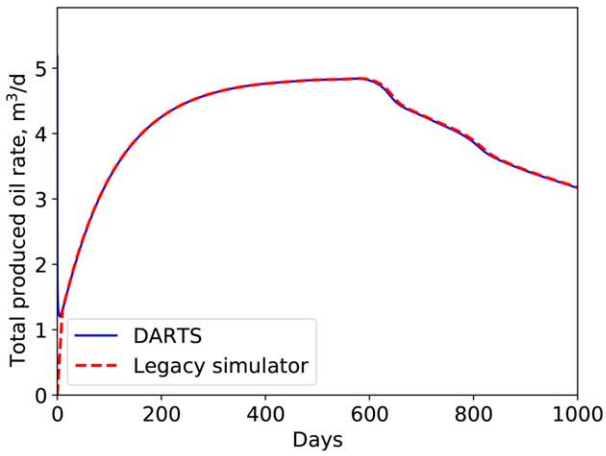

(a) Total oil production rate

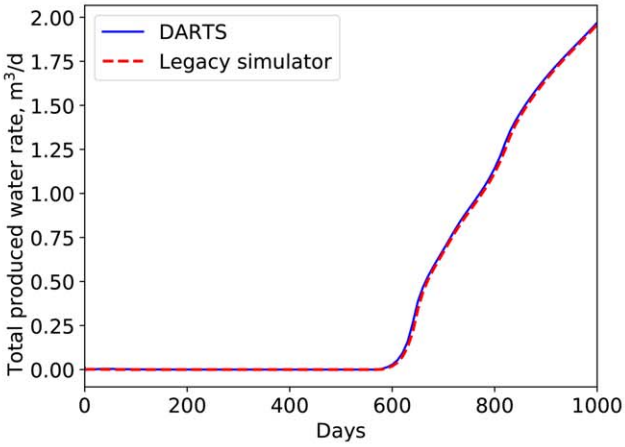

(b) Total water production rate

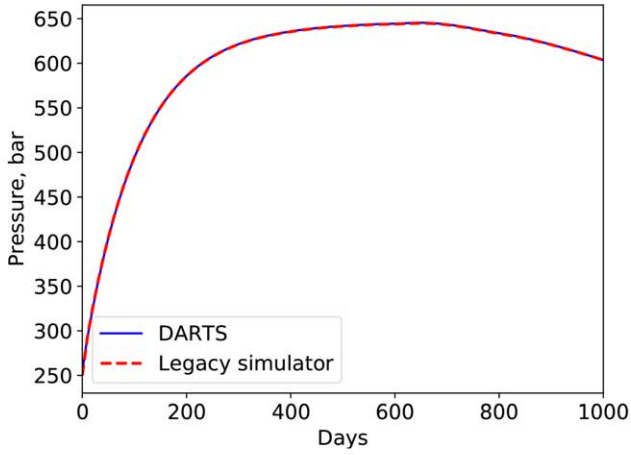

(c) Injector BHP

Fig. 17—Comparison of total production rate and injector BHP between DARTS and the legacy simulator. All rates are calculated at surface conditions.

Fig. 19a shows the performance of two simulators. In this case, DARTS takes only approximately 13 seconds, with 358 Newton iterations and 4,328 linear iterations; the legacy simulator, however, takes 24 seconds and requires 412 Newton iterations and 3,279 linear iterations. With a larger timestep ($\Delta t = 20$ days), the legacy simulator would experience convergence issues in a few timesteps. DARTS, however, is more robust and keeps the same accuracy. It indicates that the combined implementation of linear and nonlinear solution strategies using the OBL approach not only simplifies the construction of Jacobian and residual, but also significantly improves the performance of the simulation process when tackling complex physical problems.

Compositional 10th SPE Comparative Study. To further investigate the performance of the OBL approach, we run simulation for an isothermal injection of carbon dioxide (CO_2) and methane into a four-component oil using the 10th SPEcomparative study reservoir description. This model is similar to one used in Khait and Voskov (2018a). The initial oil consists of four components [i.e., CO_2 (1.0%), methane (11%), C_4 (38%), and C_{10} (50%), following Orr et al. (1995)]. The initial reservoir pressure and temperature are 90 bar and 353 K, respectively. A mixture of 80% of CO_2 and 20% of C_1 is injected from the injector in the center at a BHP control equal to 120 bar (near-miscible conditions). The four producers at the corners are operated at BHP of 60 bar. The relative permeability and capillary pressure curves for a gas/oil system are from Killough and Kossack (1987). The Peng and Robinson (1976) equation of state and the Lohrenz et al. (1964) correlations for a viscosity model are used to evaluate phase behavior and properties, the same as those in Khait and Voskov (2018a). All simulations are run for 1,000 days with a maximum timestep of $\Delta t = 10$ days. After a convergence investigation, an OBL resolution with 64 supporting points in normal space is used in this case because a relatively low resolution already provides high accuracy, as shown in Khait and Voskov (2018a), where the capillary pressure is neglected.

Fig. 20 shows the distribution of CO_2 composition and the difference between the two simulators by the end of the simulation. The difference is mainly distributed near the leading displacement shock. Fig. 19b shows the performance of two simulators. In this compositional kernel, DARTS significantly improves the performance of the simulation process compared with the dead-oil and black-oil kernels, corresponding to fewer nonlinear (510 vs. 645) and linear iterations (5,870 vs. 6,191). DARTS takes approximately 36 seconds, nearly three times faster than the legacy simulator. In DARTS, only 13,956 supporting points (0.083%) are evaluated to obtain phase properties in the simulation; the legacy simulator, however, requires 8.514×10^6 times (i.e., all blocks need to perform phase-behavior evaluations in each nonlinear iteration, which is a computationally expensive process). It further indicates the ability of the OBL approach to improve the performance of the simulation with complex physical problems.

Because of the implementation of the adaptive parametrization approach, all the computed supporting points are stored after the simulation. For the second or further runs, we can avoid property computations almost completely by loading previously computed points. This process can speed up the simulation significantly if the time cost for point generation is huge.

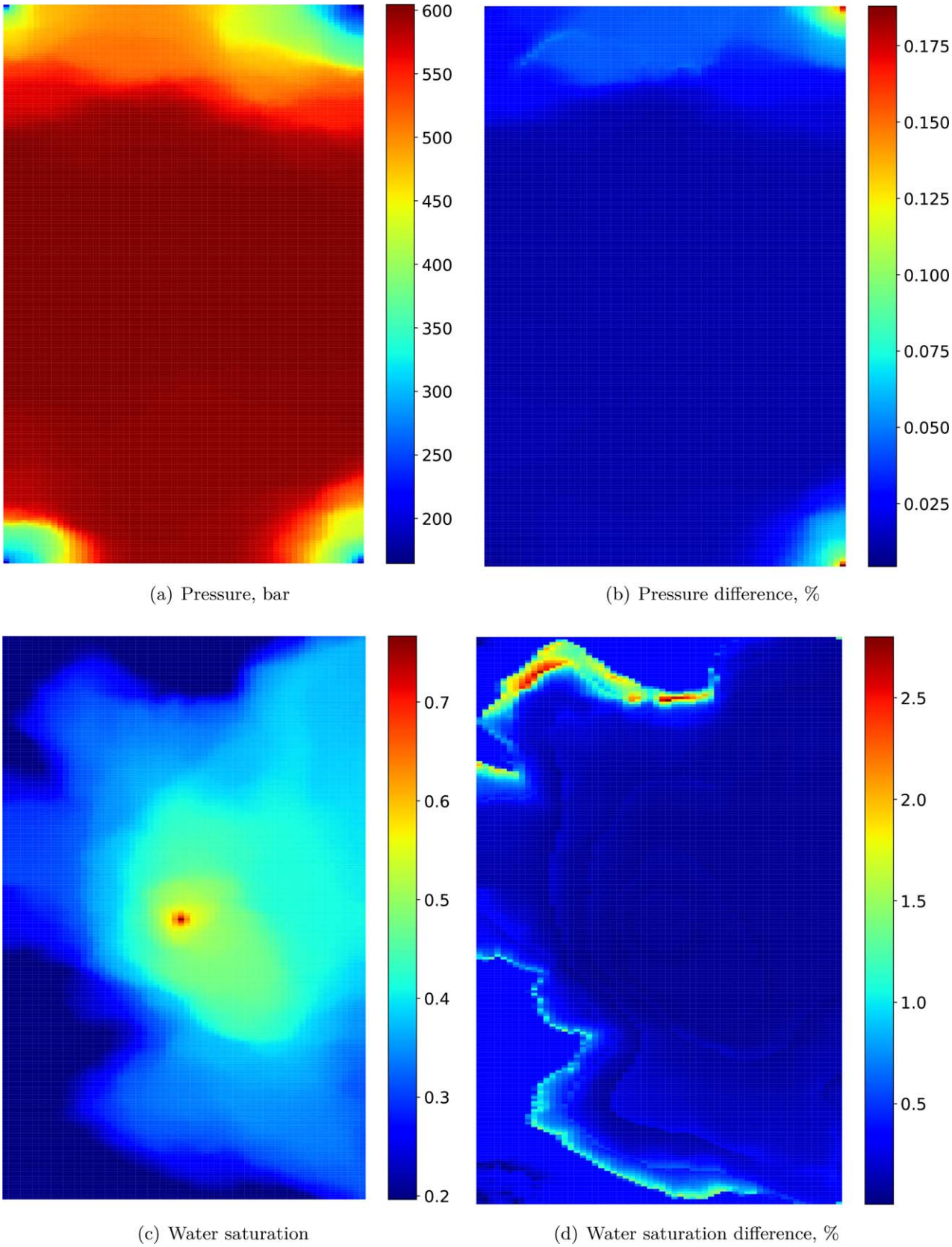

(a) Pressure, bar

(b) Pressure difference, %

(c) Water saturation

(d) Water saturation difference, %

Fig. 18—Comparison of pressure and water-saturation distribution between DARTS and the legacy simulator.

Convergence of OBL Results. **Table 2** shows the numerical convergence of DARTS on the desktop Intel® Xeon® (Intel Corporation, Santa Clara, California, USA) CPU 3.50 GHz. We perform the convergence study by setting a threshold for the difference in pressure (1%) and saturations (1%) between the exhaustive OBL resolution (10^6 points) close to the continuous physics and the OBL resolution, which provides the solution satisfying the threshold (the second column in Table 2). The last two columns show the Newton iterations of the reference case (exhaustive OBL resolution) and the current realization (OBL resolution in the second column). After the solution is lower than the threshold, the number of nonlinear iterations does not change much. In general, the black-oil kernels require a higher OBL resolution to

converge to the reference solutions because of the more nonlinear three-phase properties. In the investigated benchmark cases, the selected OBL resolution (1,000 points) always satisfies the convergence criteria. The reduced number of interpolation points can help with advanced nonlinear solvers according to a second-order analysis of parametrization tables, similar to one proposed in Pour and Voskov (2020).

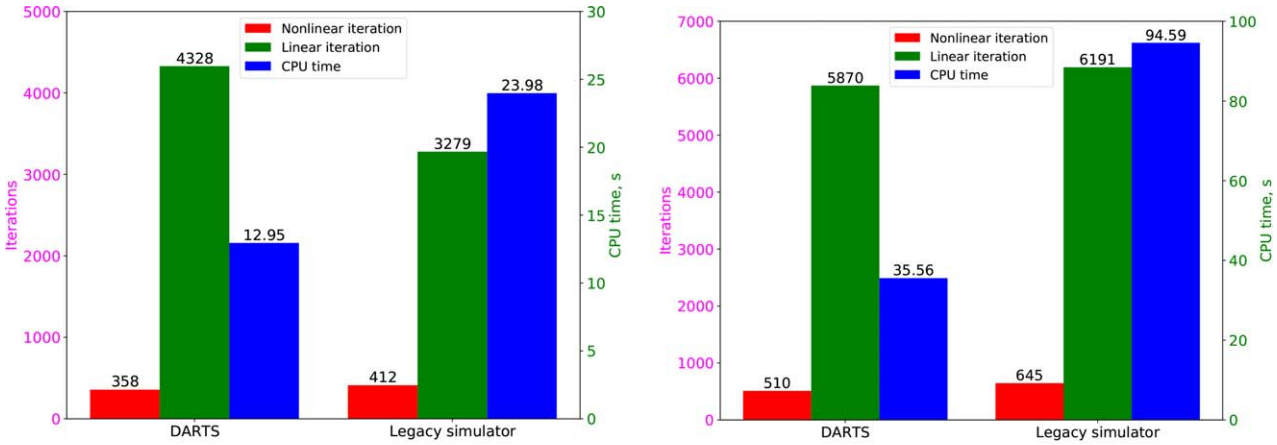

(a) Dead-oil kernel (b) Compositional kernel

Fig. 19—Performance of two simulators for the 10th SPEcomparative study model with different physics.

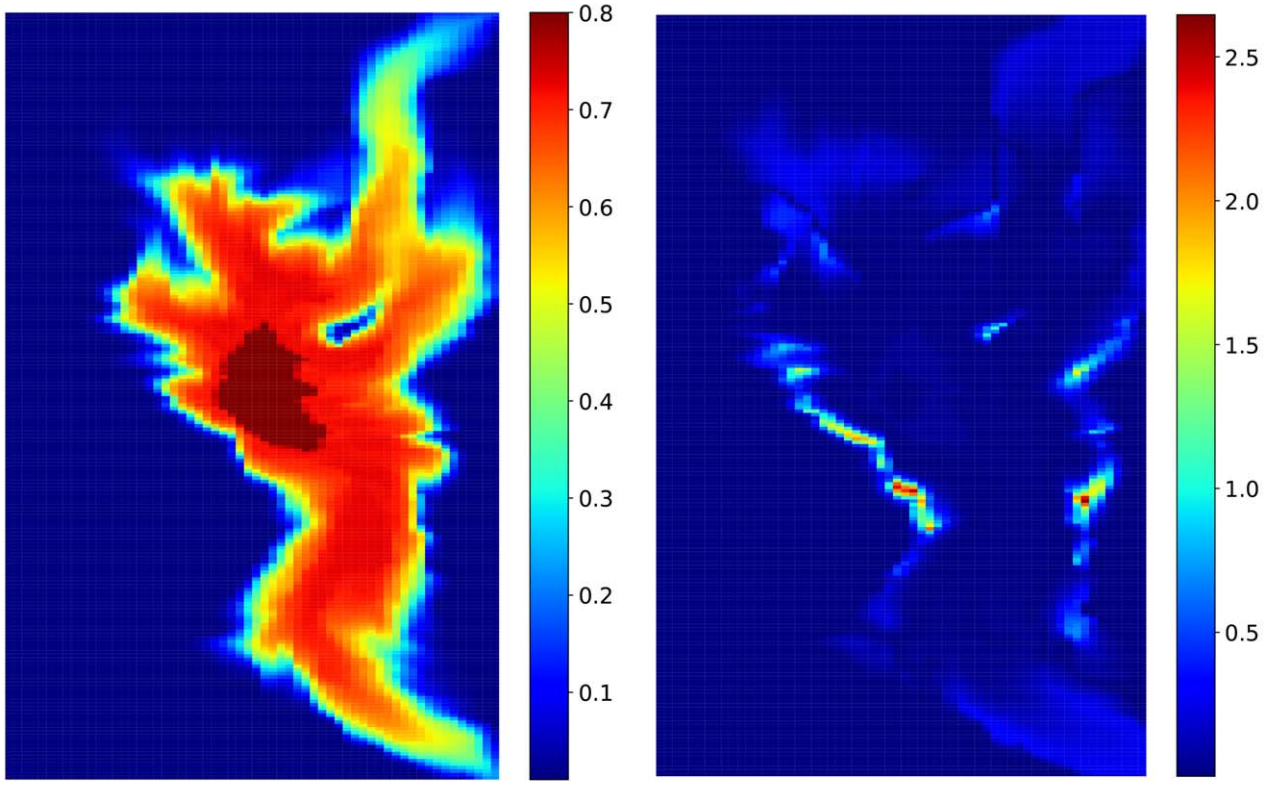

(a) CO_2 composition (b) CO_2 composition difference, %

Fig. 20—Comparison of CO_2-composition distribution between DARTS and the legacy simulator.

Scenarios	OBL Resolution	E_p (%)	E_{so} (%)	E_{sw} (%)	Newton Iterations	
					Reference	Current Realization
First SPE comparative study	220	0.313	0.854	0.466	798	804
Ninth SPE comparative study	500	0.823	0.383	0.473	383	392
UNISIM-I	680	0.473	0.285	0.330	497	506
10th SPE comparative study	20	0.012	0.028	0.042	306	298
Compositional 10th SPE comparative study	30	0.026	0.035	–	486	492

Table 2—Convergence performance of DARTS and reference.

Discussion

In this work, we extend the capacity of DARTS to the modeling of petroleum-related applications with gravity and capillarity. In the presence of buoyancy and capillarity, the nonlinearity of the system of governing equations is amplified. The newly proposed linearization approach is implemented in DARTS to control the nonlinearity of the coupled system by grouping the variables depending on the physical state into operators. These state-dependent operators are evaluated and stored at vertices of parameterization space. In the course of the simulation, a multilinear interpolation is used to interpolate the corresponding values and derivatives of operators.

Through the set of benchmark tests using dead-oil, black-oil, and compositional physical kernels, we demonstrate the high accuracy and good performance of the OBL approach to solve the problems with complex nonlinear physics. However, the following two limitations still need to be resolved in future research:

- In the current approach, the location of the supporting points is chosen according to a uniform distribution. In the black-oil kernel, gas density is usually relatively low, leading to a small gas composition of the mixtures. Therefore, the presence of gas requires a higher OBL resolution to reproduce the reference results which, in turn, increases the computational cost. The transformation of the interpolation kernel into a logarithmic scale can solve this problem to some extent. However, we still need to explore more efficient alternatives.
- In the presence of gravity and capillarity, the PPU scheme is applied in our framework to approximate the numerical flux. The number of operators involved in OBL with PPU approximation increases by $[(n_c + 1)n_p]$, which increases the computational cost, because more time is required to interpolate the values of different operators. One approach, named component-potential upwinding, which can reduce the number of operators, is proposed in Khait (2019) and will be effectively coupled with capillary operators in future research.

In simulations, the table resolution is one key factor that affects the accuracy of the OBL approach. A coarser parameterization space, corresponding to a smaller OBL resolution, usually gives a greater deviation from the conventional solution (Voskov 2017; Khait and Voskov 2018a). To choose a proper resolution, a sensitivity study is required, similar to one shown in Table 2. Note that this study can be performed on a simplified 1D model. To improve the accuracy, a higher OBL resolution can always be applied considering the efficiency of the advanced linearization scheme.

To demonstrate the ability of DARTS to perform challenging buoyancy/capillary-dominated simulation, we include only relatively simple physical kernels corresponding to the dead-oil, black-oil, and compositional physics. In the future, we will test the applicability of the OBL approach to more complicated physics describing foam-enhanced-oil-recovery and CO_2-sequestration processes where gravity and capillarity play a crucial role. Another focus of our future work is to reduce the number of operators, especially for the convective flux operators, thus improving the performance of the OBL approach. We also expect that we will be able to improve performance even further by using specifically designed nonlinear solvers for the OBL approach.

Conclusions

In this study, the ability of handling complex physical models in DARTS is investigated for several benchmark tests in the presence of buoyancy and capillarity. We compare the accuracy and computational performance of DARTS with a commercial legacy simulator widely used in the petroleum industry. The following conclusions can be made:

1. DARTS can reproduce the results of the legacy simulation with a negligible difference.
2. By approximating the reference physics using parameterization, the OBL approach simplifies the assemble of Jacobian at the linearization stage, leading to a better simulation performance.
3. In all simulation tests, starting from the 1D homogeneous model and finishing with 3D highly heterogeneous models, OBL resolution plays an important role in the accuracy of the OBL approach.
4. With increasing degrees of freedom in the simulation problem, DARTS shows its advantages to speed up the modeling process.

Nomenclature

c_r = rock compressibility, 1/bar
D = vertical depth vector (up-down oriented), m
J = Jacobian
k_{rj} = phase relative permeability
K = effective permeability tensor, m
n_c = number of components
n_p = number of phases
p_c = capillary pressure, bar
p_j = phase pressure, bar
$\tilde{q}_j$ = phase in/outflux, m^3/d
r = residual
s_j = phase saturation
u_j = phase velocity, m/d
x_{cj} = component mole fraction in a phase
α_c = physical term of mass accumulation operator, mol/m^3
β_c = physical term of mass convection operator, mol/m^3/cp
δ = mass density operator, kg/m^3
ζ = capillary operator, bar
Γ^l = geometrical part of transmissibility, cp m^3/d/bar
μ_j = phase viscosity, cp
ϕ = effective rock porosity
ρ_j = phase molar density, mol/m^3

Acknowledgments

We acknowledge the partial financial support of the China Scholarship Council (Grant No. 201706440023) and the National Priorities Research Program (Grant No. NPRP10-0208-170407) from the Qatar National Research Fund.

References

Avansi, G. D. and Schiozer, D. J. 2015. UNISIM-I: Synthetic Model for Reservoir Development and Management Applications. *International Journal of Modeling and Simulation for the Petroleum Industry* **9** (1): 21–30.

Aziz, K. and Settari, A. 1979. *Petroleum Reservoir Simulation*. London, UK: Applied Science Publishers.

Aziz, K. and Wong, T. 1989. Considerations in the Development of Multipurpose Reservoir Simulation Models. Oral presentation given at the First and Second International Forum on Reservoir Simulation, Alpbach, Austria, 12–16 September.

Brooks, R. and Corey, T. 1964. *Hydraulic Properties of Porous Media*. Fort Collins, Colorado, USA: Hydrology Papers, Colorado State University.

Cao, H. 2002. *Development of Techniques for General Purpose Simulators*. PhD dissertation, Stanford University, Stanford, California, USA (June 2002).

Chang, J. and Yortsos, Y. C. 1992. Effect of Capillary Heterogeneity on Buckley-Leverett Displacement. *SPE Res Eng* **7** (2): 285–293. SPE-18798-PA. https://doi.org/10.2118/18798-PA.

Christie, M. A. and Blunt, M. 2001. Tenth SPE Comparative Solution Project: A Comparison of Upscaling Techniques. Paper presented at the SPE Reservoir Simulation Symposium, Houston, Texas, USA, 11–14 February. SPE-66599-MS. https://doi.org/10.2118/66599-MS.

Coats, K. 1980. An Equation of State Compositional Model. *SPE J*. **20** (5): 363–376. SPE-8284-PA. https://doi.org/10.2118/8284-PA.

Coats, K. H., Thomas, L., and Pierson, R. 1995. Compositional and Black Oil Reservoir Simulation. Paper presented at the SPE Reservoir Simulation Symposium, San Antonio, Texas, USA, 12–15 February. SPE-29111-MS. https://doi.org/10.2118/29111-MS.

Edwards, M. G. and Rogers, C. F. 1998. Finite Volume Discretization with Imposed Flux Continuity for the General Tensor Pressure Equation. *Computat Geosci* **2** (4): 259–290. https://doi.org/10.1023/A:1011510505406.

Ewing, R. E. 1991. Simulation of Multiphase Flows in Porous Media. *Transp Porous Med* **6** (5–6): 479–499. https://doi.org/10.1007/BF00137846.

Garipov, T., Tomin, P., Rin, R. et al. 2018. Unified Thermo-Compositional-Mechanical Framework for Reservoir Simulation. *Computat Geosci* **22** (4): 1039–1057. https://doi.org/10.1007/s10596-018-9737-5.

Gaspar, A. T., Santos, A., Maschio, C. et al. 2015. UNISIM-I-M: Study Case for Management Variables Optimization of Reservoir Exploitation Strategy. *International Journal of Modeling and Simulation for the Petroleum Industry* **9**: 1–7.

Hamon, F. P., Mallison, B. T., and Tchelepi, H. A. 2018. Implicit Hybrid Upwinding for Two-Phase Flow in Heterogeneous Porous Media with Buoyancy and Capillarity. *Comput Methods Appl Mech Eng* **331** (1 April): 701–727. https://doi.org/10.1016/j.cma.2017.10.008.

Kala, K. and Voskov, D. 2020. Element Balance Formulation in Reactive Compositional Flow and Transport with Parameterization Technique. *Computat Geosci* **24** (2): 609–624. https://doi.org/10.1007/s10596-019-9828-y.

Khait, M. 2019. *Delft Advanced Research Terra Simulator: General Purpose Reservoir Simulator with Operator-Based Linearization*. PhD dissertation, Delft University of Technology, Delft, The Netherlands (December 2019).

Khait, M. and Voskov, D. V. 2017. Operator-Based Linearization for General Purpose Reservoir Simulation. *J Pet Sci Eng* **157** (August): 990–998. https://doi.org/10.1016/j.petrol.2017.08.009.

Khait, M. and Voskov, D. 2018a. Adaptive Parameterization for Solving of Thermal/Compositional Nonlinear Flow and Transport with Buoyancy. *SPE J*. **23** (2): 522–534. SPE-182685-PA. https://doi.org/10.2118/182685-PA.

Khait, M. and Voskov, D. 2018b. Operator-Based Linearization for Efficient Modeling of Geothermal Processes. *Geothermics* **74** (July): 7–18. https://doi.org/10.1016/j.geothermics.2018.01.012.

Khait, M., Voskov, D., and Zaydullin, R. 2020. High Performance Framework for Modelling of Complex Subsurface Flow and Transport Applications. Oral presentation given at the ECMOR XVII–17th European Conference on the Mathematics of Oil Recovery, Virtual, 14–17 September. https://doi.org/10.3997/2214-4609.202035188.

Killough, J. 1995. Ninth SPE Comparative Solution Project: A Reexamination of Black-Oil Simulation. Paper presented at the SPE Reservoir Simulation Symposium, San Antonio, Texas, USA, 12–15 February. SPE-29110-MS. https://doi.org/10.2118/29110-MS.

Killough, J. and Kossack, C. 1987. Fifth Comparative Solution Project: Evaluation of Miscible Flood Simulators. Paper presented at the SPE Symposium on Reservoir Simulation, San Antonio, Texas, USA, 1–4 February. SPE-16000-MS. https://doi.org/10.2118/16000-MS.

Li, B. and Tchelepi, H. A. 2015. Nonlinear Analysis of Multiphase Transport in Porous Media in the Presence of Viscous, Buoyancy, and Capillary Forces. *J Comput Phys* **297** (15 September): 104–131. https://doi.org/10.1016/j.jcp.2015.04.057.

Lohrenz, J., Bray, B. G., and Clark, C. R. 1964. Calculating Viscosities of Reservoir Fluids from Their Compositions. *J Pet Technol* **16** (10): 1171–1176. SPE-915-PA. https://doi.org/10.2118/915-PA.

Odeh, A. S. 1981. Comparison of Solutions to a Three-Dimensional Black-Oil Reservoir Simulation Problem (includes associated paper 9741). *J Pet Technol* **33** (1): 13–25. SPE-9723-PA. https://doi.org/10.2118/9723-PA.

Orr, F. M. Jr., Dindoruk, B., and Johns, R. T. 1995. Theory of Multicomponent Gas/Oil Displacements. *Ind. Eng. Chem. Res.* **34** (8): 2661–2669. https://doi.org/10.1021/ie00047a015.

Peaceman, D. 1977. A Nonlinear Stability Analysis for Difference Equations Using Semi-Implicit Mobility. *SPE J*. **17** (1): 79–91. SPE-5735-PA. https://doi.org/10.2118/5735-PA.

Peaceman, D. W. 2000. *Fundamentals of Numerical Reservoir Simulation*, Vol. 6, first edition. New York, New York, USA: Elsevier.

Peng, D.-Y. and Robinson, D. B. 1976. A New Two-Constant Equation of State. *Ind. Eng. Chem. Fundamen.* **15** (1): 59–64. https://doi.org/10.1021/i160057a011.

Pour, K. M. and Voskov, D. 2020. Adaptive Nonlinear Solver for a Discrete Fracture Model in Operator-Based Linearization Framework. Oral presentation given at ECMOR XVII–17th European Conference on the Mathematics of Oil Recovery, Virtual, 14–17 September. https://doi.org/10.3997/2214-4609.202035094.

Saad, Y. 1993. A Flexible Inner-Outer Preconditioned GMRES Algorithm. *SIAM J. Sci. Comput.* **14** (2): 461–469. https://doi.org/10.1137/0914028.

Saad, Y. and Schultz, M. H. 1986. GMRES: A Generalized Minimal Residual Algorithm for Solving Nonsymmetric Linear Systems. *SIAM J. Sci. Comput.* **7** (3): 856–869. https://doi.org/10.1137/0907058.

Spillette, A., Hillestad, J., and Stone, H. 1973. A High-Stability Sequential Solution Approach to Reservoir Simulation. Paper presented at the Fall Meeting of the Society of Petroleum Engineers of AIME, Las Vegas, Nevada, USA, 30 September–3 October. SPE-4542-MS. https://doi.org/10.2118/4542-MS.

Thomas, G. and Thurnau, D. 1983. Reservoir Simulation Using an Adaptive Implicit Method. *SPE J*. **23** (5): 759–768. SPE-10120-PA. https://doi.org/10.2118/10120-PA.

Todd, M. R., O'Dell, P. M., and Hirasaki, G. J. 1972. Methods for Increased Accuracy in Numerical Reservoir Simulators. *SPE J*. **12** (6): 515–530. SPE-3516-PA. https://doi.org/10.2118/3516-PA.

Voskov, D. V. 2017. Operator-Based Linearization Approach for Modeling of Multiphase Multi-Component Flow in Porous Media. *J Comput Phys* **337** (15 May): 275–288. https://doi.org/10.1016/j.jcp.2017.02.041.

Voskov, D. V. and Tchelepi, H. A. 2012. Comparison of Nonlinear Formulations for Two-Phase Multi-Component EoS Based Simulation. *J Pet Sci Eng* **82–83** (February–March): 101–111. https://doi.org/10.1016/j.petrol.2011.10.012.

Wallis, J. R., Kendall, R., and Little, T. 1985. Constrained Residual Acceleration of Conjugate Residual Methods. Paper presented at the SPE Reservoir Simulation Symposium, Dallas, Texas, USA, 10–13 February. SPE-13536-MS. https://doi.org/10.2118/13536-MS.

Wang, Y., Voskov, D., Khait, M. et al. 2020. An Efficient Numerical Simulator for Geothermal Simulation: A Benchmark Study. *Appl Energy* **264** (15 April): 114693. https://doi.org/10.1016/j.apenergy.2020.114693.

Young, L. and Russell, T. 1993. Implementation of an Adaptive Implicit Method. Paper presented at the SPE Symposium on Reservoir Simulation, New Orleans, Louisiana, USA, 28 February–3 March. SPE-25245-MS. https://doi.org/10.2118/25245-MS.

Younis, R. M. 2011. *Modern Advances in Software and Solution Algorithms for Reservoir Simulation*. PhD dissertation, Stanford University, Stanford, California, USA (August 2011).

Zaydullin, R., Voskov, D., and Tchelepi, H. A. 2013. Nonlinear Formulation Based on an Equation-of-State Free Method for Compositional Flow Simulation. *SPE J*. **18** (2): 264–273. SPE-146989-PA. https://doi.org/10.2118/146989-PA.

Zaydullin, R., Voskov, D., and Tchelepi, H. 2016. Phase-State Identification Bypass Method for Three-Phase Thermal Compositional Simulation. *Computat Geosci* **20** (3): 461–474. https://doi.org/10.1007/s10596-015-9510-y.